Journal of Power Sources 195 (2010) 2608–2612

Contents lists available at ScienceDirect

Journal of Power Sources

journal homepage: www.elsevier.com/locate/jpowsour

Short communication

Visualization of invasion–percolation drainage process in porous media using density-matched immiscible fluids and refractive-index-matched solid structures

Jung Ho Kang[a], Kyu-Jin Lee[a], Jin Hyun Nam[b,*], Charn-Jung Kim[a], Hee Sung Park[c], Sungho Lee[c], Inchul Kwang[c]

[a] School of Mechanical and Aerospace Engineering, Seoul National University, Seoul 151-742, Republic of Korea
[b] School of Mechanical and Automotive Engineering, Kookmin University, Seoul 136-702, Republic of Korea
[c] Research and Development Division, Hyundai-Kia Motors Co., Yongin 446-912, Republic of Korea

ARTICLE INFO

Article history:
Received 28 August 2009
Received in revised form 8 October 2009
Accepted 16 November 2009
Available online 26 November 2009

Keywords:
Polymer electrolyte membrane fuel cell
Gas-diffusion layer
Liquid water transport
Similarity model experiment
Invasion–percolation
Capillary fingering

ABSTRACT

Liquid water transport in hydrophobic gas-diffusion layers (GDLs) of polymer electrolyte membrane fuel cells (PEMFCs) is indirectly investigated through a similarity model experiment, that visualizes the drainage process in a porous layer. The dimensionless parameters for the visualization experiment are controlled to be close to those for liquid water transport in hydrophobic GDLs by slowly injecting a density-matched immiscible fluid into a porous layer saturated with liquid water. The visual inspection of the drainage process is conducted by constructing the porous layer with saturated hydrogel spheres possessing a refractive index that is almost the same as that of liquid water. The visualization results indicate that the drainage process considered in this study is a strongly capillary-driven process governed by invasion–percolation, this suggests that invasion–percolation with capillary dendrite-like penetration (fingering) can also be an important mechanism of liquid water transport in hydrophobic GDLs. The study also examines the morphological similarities between the non-wetting fluid distribution observed for the present drainage experiment and that predicted by a steady pore-network model for liquid water transport in hydrophobic GDLs.

1. Introduction

Polymer electrolyte membrane fuel cells (PEMFCs) are energy conversion devices that directly generate electricity by the electrochemical combination of hydrogen and oxygen while simultaneously producing water and heat as reaction by-products [1,2]. Condensed water in catalyst layers (CLs), gas-diffusion layers (GDLs), and gas channels (GCs) is known to result in lower performance of PEMFCs by increasing mass transport resistances or activation overpotentials. Thus, improved water management is considered to be a crucial issue for enhancing the performance of PEMFCs [3,4]; however, the water transport and flooding behavior in porous layers of PEMFCs have been experimentally observed by only a number of researchers. This is due to the technical difficulties related to observing liquid water transport and measuring its saturation distribution during the actual operation of PEMFCs [5].

The visualization of liquid water transport in hydrophobic GDLs is a challenging task, mainly due to their very small thicknesses of only around 200 μm. Environmental scanning electron microscopy (ESEM) has been used for ex-situ qualitative observation of the condensation and evolution of liquid water in hydrophobic GDLs [6], CLs [7,8], and microporous layers [9]. Litster et al. [10] used fluorescence microscopy for ex-situ visualization of through-plane liquid water transport in carbon paper GDLs. Later, this visualization technique was employed to investigate the effect of GDL compression on liquid water transport [11] and to characterize the dynamics of droplet emergence from GDLs [12]. High-resolution neutron radiography has been recently used for in-situ quantitative measurement of the through-plane liquid water content in the GDLs of operating PEMFCs [13,14]. All of these visualization and measurement results show that the microscale capillary process is important for liquid water transport in GDLs.

Recent pore-network studies have also suggested that liquid water transport in hydrophobic GDLs is a strongly capillary-driven process [15–19]. The liquid water saturation distribution in GDLs predicted by pore-network models is quite different from that predicted by continuum two-phase flow models. It should be noted that the pore-network results reported in [15–19] are more

* Corresponding author at: 861-1 Jeongneung-dong, Seongbuk-gu, Seoul 136-702, Republic of Korea. Tel.: +82 2 910 4858; fax: +82 2 910 4839.
E-mail address: akko2@kookmin.ac.kr (J.H. Nam).

0378-7753/$ – see front matter © 2009 Elsevier B.V. All rights reserved.
doi:10.1016/j.jpowsour.2009.11.087

consistent with the phase diagram for the two-phase drainage flow proposed by Lenormand et al. [20]. Drainage denotes a situation in which a non-wetting phase (liquid water) invades a porous medium (a GDL) by displacing the initially residing wetting phase (air). According to Lenormand et al. [20], invasion–percolation with active capillary fingering is expected to be the main mechanism of liquid water transport in hydrophobic GDLs. In order to verify the validity of the pore-network results, a more detailed inspection or visualization of liquid water transport in hydrophobic GDLs is required. This may be alternatively achieved by a similarity model experiment [21] with dimensionless parameters that characterize two-phase flow behavior being and are closely matched to those of liquid water transport in GDLs.

In this study, a similarity model experiment is developed for indirect investigation of liquid water transport in hydrophobic GDLs. Three dimensionless parameters, i.e., the capillary number, viscosity ratio, and bond number, of the model experiment are controlled to be close to those encountered during the operation of PEMFCs. The refractive index of solid structures (hydrogel spheres) in the model porous layer is matched to that of a defending wetting fluid (liquid water) for visual inspection of the internal transport process. The density of an invading non-wetting fluid (a dyed mixture of soy-bean oil and carbon tetrachloride) is also matched to that of liquid water to minimize gravitational effects. In the visualization experiment, the invading non-wetting fluid is injected at a very small flow rate (20 ml h^{-1}) into the hydrogel layer initially saturated with liquid water. Then, the evolution of the non-wetting fluid distribution is photographed.

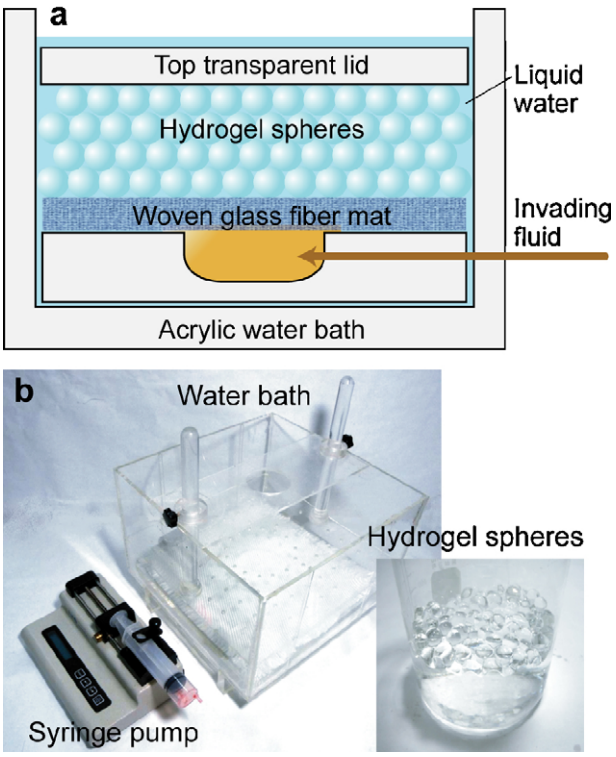

Fig. 1. Experimental setup for similarity model experiment visualizing the drainage process in a porous layer: (a) schematic diagram, and (b) component pictures.

2. Experimental

A schematic diagram for the similarity model experiment is provided in Fig. 1, along with photographs that show the actual components used in the experiment. In order to construct a model porous layer that simulates hydrophobic GDLs, saturated hydrogel spheres of about 1 cm in diameter were randomly packed to a height of 7 cm inside a transparent acrylic bath (base area of 30 cm by 30 cm). When liquid water (a defensive wetting fluid) completely filled the pores between the hydrogel spheres, the hydrogel layer and liquid water appeared as clear water with almost invisible interfaces. This is because hydrogel spheres contain more than 95 vol.% of liquid water when fully saturated; therefore, their refractive index is almost the same as that of liquid water. Thus, it was possible to inspect visually the transport process inside the porous layer of the hydrogel spheres.

At the top of the hydrogel layer, a transparent lid was placed to fix the hydrogel spheres which are neutrally buoyant in liquid water. Small holes were made in the lid to permit the exhaust of liquid water from the hydrogel layer due to the injection of a non-wetting fluid. The hydrogel spheres exhibited some elasticity when compressed by the top lid, but the anisotropy of the pore structures in the hydrogel layers is believed to be small. At the bottom of the bath, a circular hole of 10 cm in diameter was made for the injection of a non-wetting fluid. This circular injection hole was fully covered with a fine porous layer (5 mm thickness) made of a woven glass-fibre mat. The layer ensured spatially uniform invasion of the non-wetting fluid into the hydrogel layer. Thus, the layer simulated the uniform generation of liquid water in CLs and subsequent breakthrough into hydrophobic GDLs. The geometrical parameters for the porous layers used in the experiment are summarized in Table 1.

A dyed mixture of soy-bean oil and carbon tetrachloride (CCl_4) was used as the invading non-wetting fluid. This liquid mixture is immiscible with liquid water and has almost the same density as liquid water. The density matching was assured by visually checking the neutrally buoyant behavior of the non-wetting fluid droplets in liquid water. The experiment was initiated by injecting the density-matched liquid mixture through the circular injection hole into a hydrogel layer initially filled with liquid water. Then, photographs were taken at constant intervals to record the transport behaviors of the non-wetting fluid during invasion into the transparent hydrogel layer. A very low injection rate of 20 ml h^{-1} (0.67 ml min^{-1}) was maintained by means of a syringe pump (Model 781100, KD Scientific, Holliston, MA), which corresponds to a constant invasion flux, q_{inv}, of 7.1×10^{-7} m s^{-1}. The operating conditions and dimensionless parameters for the visualization experiment are given in Table 2

. A typical experimental run lasted for 6–8 h before the non-wetting fluid reached the top transparent lid or a wall of the bath.

3. Results and discussion

Before presenting the visualization results, it is worth reviewing the implications of the operating conditions and dimensionless parameters provided in Table 2. Lenormand et al. [20] showed

Table 1
Geometrical parameters for porous layers used in the similarity model experiment.

Layer	Particle size	Porosity	Thickness	Counterpart in PEMFC
Glass-fibre layer	100 μm (cylindrical)	0.7	5 mm	CL
Hydrogel layer	9–10 mm (spherical)	0.4[a]	7 cm	GDL

[a] Assumed value for randomly packed spheres

Table 2
Summary of properties, operational conditions, and dimensionless parameters for similarity model experiment.

Parameters	PEMFC at 70 °C (2 A cm^{-2})	Experiment at 20 °C
Invading non-wetting fluid	Liquid water	Mixture of oil and CCl_4
Density, ρ_{inv}	977.8 kg m^{-3}	999.2[a] kg m^{-3}
Viscosity, μ_{inv}	0.000404 Pa s	0.03[b] Pa s
Defending wetting fluid	Saturated air (31 vol.% H_2O)	Liquid water
Density, ρ_{def}	0.914 kg m^{-3}	998.2 kg m^{-3}
Viscosity, μ_{def}	0.0000176 Pa s	0.001 Pa s
Interfacial properties		
Surface tension, σ	0.0645 N m^{-1}	0.0569[c] N m^{-1}
Contact angle, θ_c	120°	180[d]°
Invasion volume flux, q_{inv}	1.9 μm s^{-1}	0.71 μm s^{-1}
Mean pore diameter, d_p	20 μm	4.44[e] mm
Dimensionless parameters		
Capillary number, $Ca = \mu_{inv} q_{inv}/\sigma \cos\theta_c$	2.4×10^{-8}	3.7×10^{-7}
Viscosity ratio, $M_v = \mu_{inv}/\mu_{def}$	23	30
Bond number, $Bo = \Delta\rho g d_p^2/\sigma \cos\ \theta_c$	5.9×10^{-5}	5.5×10^{-3}[f]

[a] Density matched to liquid water.
[b] Measured value (ARES, TA instruments, New Castle, DE).
[c] Calculated by $\sigma = \sigma_{inv} + \sigma_{def} - 2a\sqrt{\sigma_{inv}\sigma_{def}}$ with $a = 0.5$; surface tension of oil–CCl_4 mixture was measured to be $\sigma_{inv} = 0.035$ N m^{-1} (Tensiomat Model 21, Fisher Scientific, Hampton, NH); surface tension of liquid water set as $\sigma_{def} = 0.072$ N m^{-1} at 20 °C.
[d] Assumed based on existence of a thin liquid water film between the hydrogel surface and non-wetting fluid.
[e] Calculated by $d_p = 2\varepsilon d/3(1-\varepsilon)$ with $\varepsilon = 0.4$ and $d = 10$ mm.
[f] Calculated with an assumed density difference, $\Delta\rho$, of 1 kg m^{-3}.

that two-phase drainage flow in porous media is governed by the capillary number, Ca, and the viscosity ratio, M_v. The capillary number is a measure of the relative importance of viscous forces with respect to capillary forces, defined as $Ca = \mu_{inv} q_{inv}/\sigma \cos\theta_c$. In ordinary operation of PEMFCs, the capillary number is very small, i.e., around 10^{-8}, primarily due to the very low generation rate of liquid water in CLs ($q_{inv} = 1.9$ μm s^{-1} for a current density of 2 A cm^{-2}). Thus, capillary effects are expected to be dominant over viscous effects for liquid water transport in the hydrophobic GDLs of PEMFCs, and have been demonstrated numerically by pore-network studies [15–19].

The capillary number in the visualization experiment was controlled to be as small as 3.7×10^{-7} by injecting the non-wetting fluid at a small flow rate of 20 ml h^{-1} ($q_{inv} = 0.71$ μm s^{-1}). It should be noted that the capillary number in the experiment is one order of magnitude larger than that under PEMFC conditions. Nevertheless, the capillary number of 3.7×10^{-7} is found to be sufficient to ensure the dominance of capillary effects. The viscosity ratio in the visualization experiment is similar to that in PEMFCs, and the bond number is sufficiently small to minimize gravitational effects.

Consecutive photographs taken from the top are presented in Fig. 2 , where the initial stage of the non-wetting fluid invasion into the hydrogel layer is well observed. The texture shown in Fig. 2 is of the woven glass-fibre mat with a fine pore structure. Spatially uniform injection of the non-wetting fluid is guaranteed by the large difference in the capillary pressure levels of the two porous layers. According to $P_c = 4\sigma\cos\theta_c/d_c$, the capillary pressure level is estimated to be about 1000 Pa for the glass-fibre layer ($d_p = \varepsilon d_f/(1-\varepsilon) = 233$ μm) and about 51 Pa for the hydrogel layer ($d_p = 4.44$ mm).

The photograph in Fig. 2(a) clearly shows that very small droplets are uniformly distributed in the circular injection region over the woven glass-fibre mat. These small droplets coalesce into larger droplets to fill the pores between the hydrogel spheres, and larger droplets further grow and are connected with other droplets in neighbouring pores, as shown in Fig. 2(b) and (c). Afterwards, the non-wetting fluid begins to penetrate into the hydrogel layer and is, driven towards larger pores with small capillary pressures, as shown in Fig. 2(d). It should be noted that the regions of darker

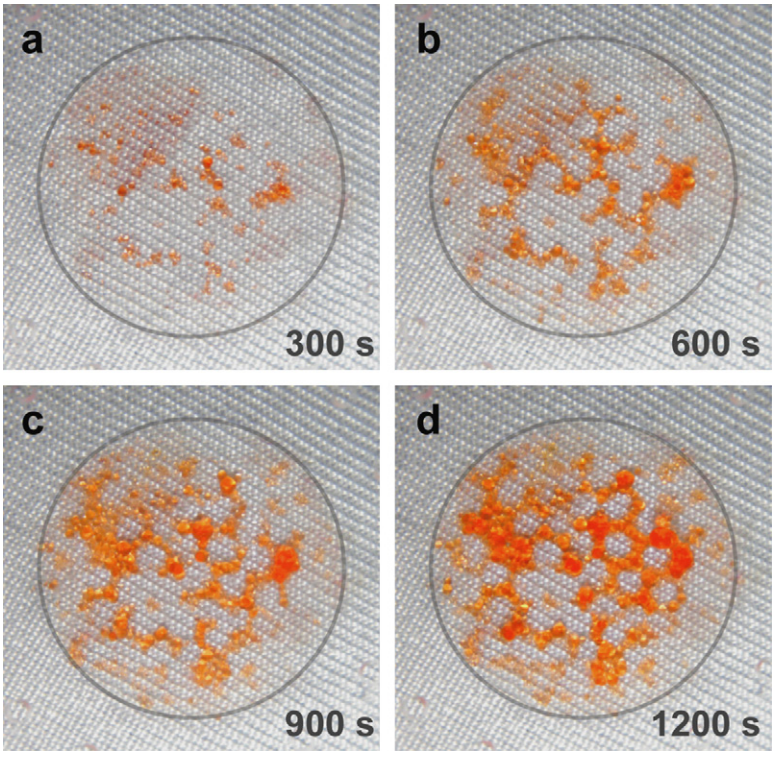

Fig. 2. Photographs taken from top of bath at (a) 300 s, (b) 600 s, (c) 900 s, and (d) 1200 s, which show initial stages of non-wetting fluid invasion into hydrogel layer.

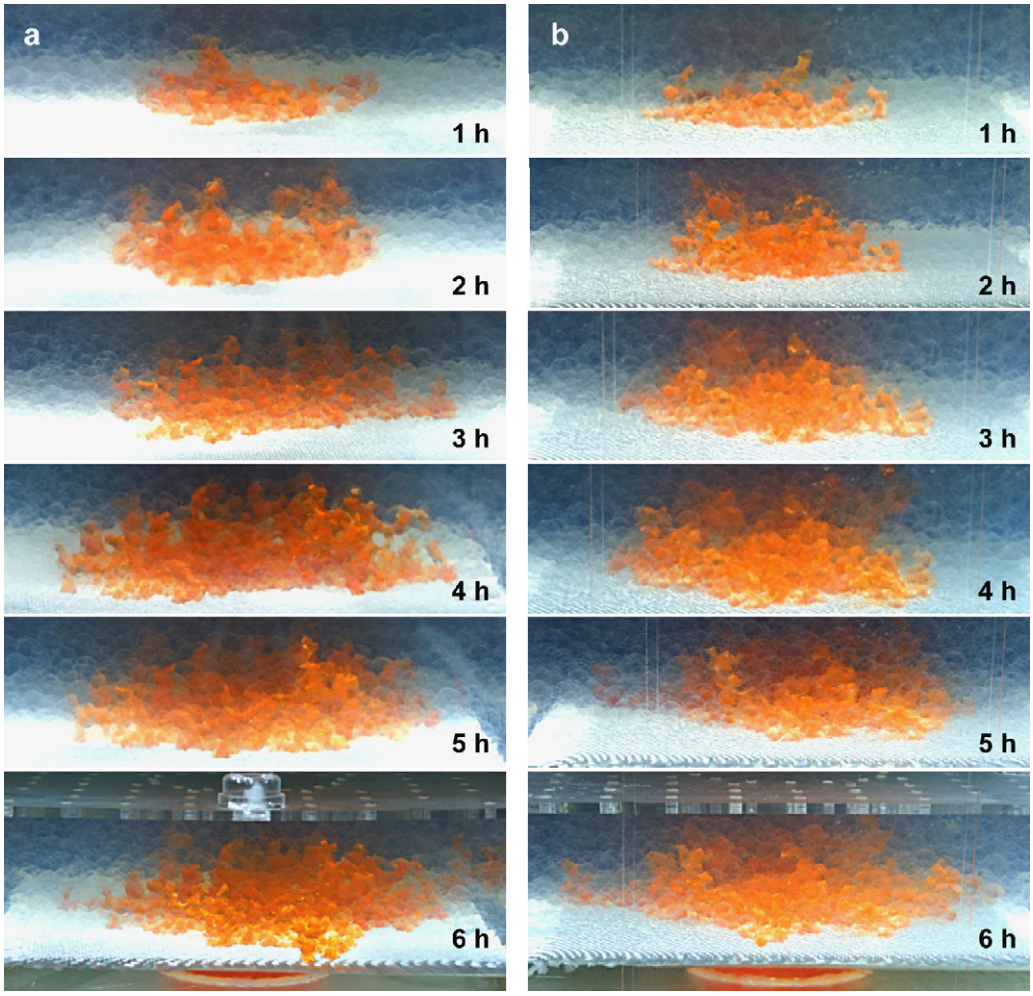

Fig. 3. Photographs taken from side of the bath at (a) 1 h, (b) 2 h, (c) 3 h, (d) 4 h, (e) 5 h, and (f) 6 h, which show the evolution of non-wetting fluid distribution in a hydrogel layer due to invasion–percolation with capillary fingering.

colour indicate where the non-wetting fluid content is higher with more active invasion. The circular shapes of the transparent hydrogel spheres are also identified in Fig. 2(d).

In Fig. 3, the evolution of the non-wetting fluid distribution due to the random invasion process is presented at constant intervals of 1 h. The photographs clearly indicate that transport of the non-wetting fluid occurs through a process of invasion–percolation with capillary fingering. Paths with larger pores (smaller capillary pressures) are invaded preferentially, which leads to very complex interface shapes in the hydrogel layer. Further injection of the non-wetting fluid expands the invaded region in the hydrogel layer, but the interface shape remains very complex due to active capillary fingering. This result is consistent with the phase diagram for two-phase drainage flow in porous media that was proposed by Lenormand et al. [20]. For capillary numbers less than 10^{-6}, the two-phase drainage flow falls in the region of capillary fingering when the viscosity ratio is larger than 1. Therefore, the two-phase drainage process shown in Fig. 3 indirectly demonstrates that liquid water transport in hydrophobic GDLs can also be governed by invasion-percolation with capillary fingering.

The capillary pressure level in the hydrogel layer is estimated to be only around 51 Pa, which is much smaller than that in hydrophobic GDLs of about 6400 Pa (d_p = 20 μm). The low capillary pressure level in the hydrogel layer used in the experiment caused the non-wetting fluid to be very susceptible to external disturbances such as impacts, vibrations, etc. For example, small unintended impacts during the experiment could induce motion or even morphological changes of the non-wetting fluid. Nevertheless, liquid water in hydrophobic GDLs is not expected to be significantly influenced by external disturbances due to its higher capillary pressure level.

Although not presented in Fig. 3, only 1–3 breakthrough paths for the non-wetting fluid exhaust are observed to form at the end of the visualization experiment. Further injection after breakthrough events results in only a small morphological change in the non-wetting fluid distribution. In fact, the interface of the non-wetting fluid and liquid water appears to be almost stationary, whereas the breakthrough droplets formed on top of the transparent lid are growing. It is also predicted by pore-network models [15–19] that the liquid water saturation distribution in hydrophobic GDLs becomes stationary once a steady state is reached.

Pore-network simulations were also conducted to investigate the similarities between the liquid water transport in hydrophobic GDLs and the non-wetting phase transport in the present experiment. The steady pore-network model proposed by Lee et al. [19] was used, but the viscous flow calculation was omitted to consider pure invasion–percolation transport (Ca = 0). The results in Lee et al. [19] showed that viscous flow effects do not significantly influence the liquid water saturation distribution in GDLs at a current density of around 2 A cm^{-2}. The size of the pore-network realizations was 1050 μm × 1050 μm × 225 μm (42 × 42 × 9 in pore numbers) to achieve geometrical similarity of the simulated and experimental domains. Liquid water was assumed to be injected through 25%

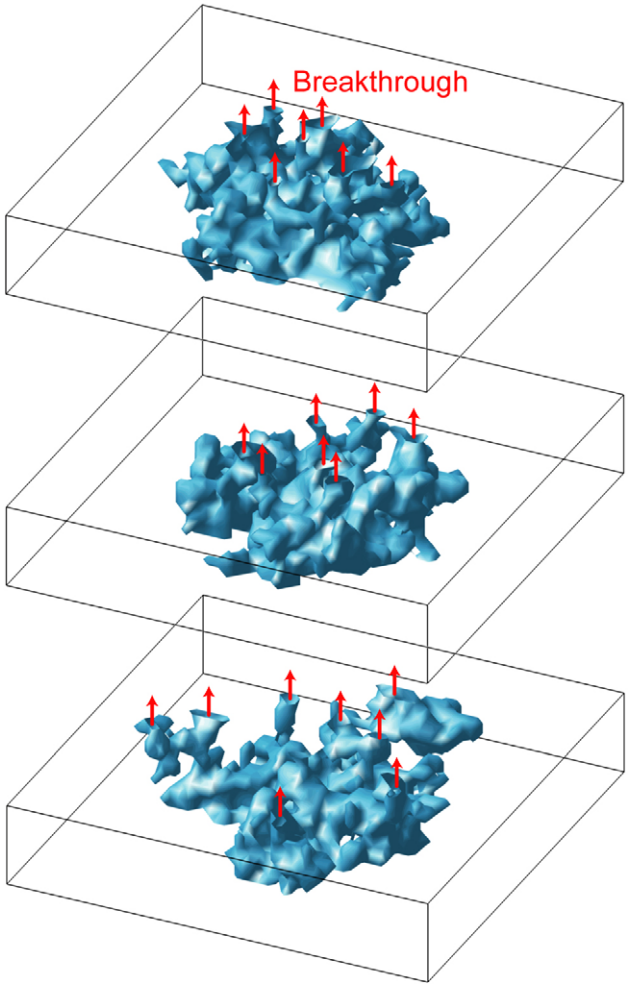

Fig. 4. Simulated saturation distribution of liquid water in hydrophobic GDLs obtained by a steady pore-network model [19].

of the inlet pores in a bottom circular region of 350 μm in diameter (14 in pore number units).

Fig. 4 shows the approximate regions of steady liquid water saturation in three different randomly generated, pore-network realizations (refer to Lee et al. [19] for the interpretation of Fig. 4). The close similarity between the simulated liquid water morphology in GDLs in Fig. 4 and the experimental non-wetting fluid distribution in Fig. 3 should be noted. Complex interface shapes due to active capillary fingering are readily observed in Fig. 4. The number of breakthrough paths is found to be 7–9 in the pore-network simulations, which is somewhat larger than that observed in the visualization experiment. The morphological similarity between the morphologies (Figs. 3 and 4) also demonstrates that invasion–percolation with capillary fingering can be an important mechanism of liquid water transport in hydrophobic GDLs.

4. Conclusion

For the investigation of liquid water transport in hydrophobic GDLs of PEMFCs, a similarity model experiment has been developed using density-matched immiscible fluids and refractive-index-matched solid structures. The two-phase flow regime of the model experiment is ensured to be similar to that of liquid water transport in hydrophobic GDLs by controlling the capillary number, viscosity ratio, and bond number. The visualization experiment shows that the non-wetting fluid transport is strongly governed by invasion–percolation with active capillary fingering. It is also demonstrated that there exists a strong similarity between the experimental non-wetting fluid distribution and the liquid water morphology in GDLs predicted by a steady pore-network model. These results suggest that invasion–percolation can also be an important mechanism of liquid water transport in hydrophobic GDLs of PEMFCs. In addition, the visualization technique is expected to be a useful tool for investigating liquid water transport in hydrophobic GLDs, as well as in other two-phase transport processes in porous media.

Acknowledgements

This work was supported by Hyundai-Kia Motors Co. through Next Generation Vehicle Technology Co. (NGVTEK.com). The authors also acknowledge Hankuk Fiber Glass Co. for providing the woven glass-fibre mat.

References

[1] A. Dicks, J. Larminie, Fuel Cell Systems Explained, second ed., John Wiley & Sons, New York, 2003.
[2] R. O'Hayre, S.W. Cha, W. Colella, F.B. Prinz, Fuel Cell Fundamentals, John Wiley & Sons, New York, 2005.
[3] H. Li, Y. Tang, Z. Wang, Z. Shi, S. Wu, D. Song, J. Zhang, K. Fatih, J. Zhang, H. Wang, Z. Liu, R. Abouatallah, A. Mazza, J. Power Sources 178 (2008) 103–117.
[4] N. Yousfi-Steiner, Ph. Moçotéguy, D. Candusso, D. Hissel, A. Hernandez, A. Aslanides, J. Power Sources 183 (2008) 260–274.
[5] A. Bazylak, Int. J. Hydrogen Energy 34 (2009) 3845–3857.
[6] J.H. Nam, M. Kaviany, Int. J. Heat Mass Transfer 46 (2003) 4595–4611.
[7] H.M. Yu, J.O. Schumacher, M. Zobel, C. Hebling, J. Power Sources 145 (2005) 216–222.
[8] H.M. Yu, C. Ziegler, M. Oszcipok, M. Zobel, C. Hebling, Electrochim. Acta 51 (2006) 1199–1207.
[9] J.H. Nam, K.J. Lee, G.S. Hwang, C.J. Kim, M. Kaviany, Int. J. Heat Mass Transfer 52 (2009) 2779–2791.
[10] S. Litster, D. Sinton, N. Djilali, J. Power Sources 154 (2006) 95–105.
[11] A. Bazylak, D. Sinton, Z.S. Liu, N. Djilali, J. Power Sources 163 (2007) 784–792.
[12] A. Bazylak, D. Sinton, N. Djilali, J. Power Sources 176 (2008) 240–246.
[13] M.A. Hickner, N.P. Siegel, K.S. Chen, D.S. Hussey, D.L. Jacobson, M. Arif, J. Electrochem. Soc. 155 (2008) B427–B434.
[14] C. Hartnig, I. Manke, R. Kuhn, N. Kardjilov, J. Banhart, W. Lehnert, Appl. Phys. Lett. 92 (2008) 134106.
[15] P.K. Sinha, C.Y. Wang, Electrochim. Acta 52 (2007) 7936–7945.
[16] P.K. Sinha, C.Y. Wang, Chem. Eng. Sci. 63 (2008) 1081–1091.
[17] K.J. Lee, J.H. Nam, C.J. Kim, Electrochim. Acta 54 (2009) 1166–1176.
[18] M. Rebai, M. Prat, J. Power Sources 192 (2009) 534–543.
[19] K.J. Lee, J.H. Nam, C.J. Kim, J. Power Sources 195 (2010) 130–141.
[20] R. Lenormand, E. Touboul, C. Zarcone, J. Fluid Mech. 189 (1988) 165–187.
[21] O. Chapuis, M. Prat, M. Quintard, E. Chane-Kane, O. Guillot, N. Mayer, J. Power Sources 178 (2008) 258–268.